Balancing Strength and Extreme Thermal Resilience in Lunar Regolith Composites: The Role of Multi-Walled Carbon Nanotubes

*Andrea J. Hoe, Amirreza Tarafdar, Wenhua Lin, Michael R. Fiske, Jennifer Edmunson, Yeqing Wang**

Andrea J. Hoe, Amirreza Tarafdar, Wenhua Lin, Yeqing Wang
Department of Mechanical and Aerospace Engineering, Syracuse University, Syracuse, NY 13244, USA
E-mail: ywang261@syr.edu

Michael R. Fiske
Amentum Space Exploration Division serving NASA MSFC, Huntsville, Alabama 35806, USA

Jennifer Edmunson
NASA Marshall Space Flight Center, Huntsville, AL 35812, USA

Abstract

The National Aeronautics and Space Administration's (NASA) Artemis program stands at the forefront of commercial space initiatives, aiming to establish sustainable lunar habitats, demanding resilient construction materials with minimal reliance on Earth-based resources. In response to these demands, this study explores the feasibility of reinforcing lunar regolith with multi-walled carbon nanotubes (MWCNTs) while relying on minimal water and additives for composite fabrication as a potential solution for building semi-permanent Moon bases. Composites incorporating 0.00 wt%, 0.25 wt%, 0.50 wt%, and 1.00 wt% MWCNTs were subjected to freeze-thaw cycles, vacuum pressures, ambient environments, and oven-curing methods to emulate the Moon's harsh environment. Results show that ambient-cured composites containing MWCNTs achieved compressive strengths exceeding 35 MPa achieving a 44.44% increase compared to the sample without MWCNTs, highlighting the reinforcing potential of carbon nanotubes (CNTs) for extraterrestrial applications. However, thermal cycling revealed performance limitations due to mismatched coefficients of thermal expansion between MWCNTs and the regolith matrix, causing microcracking. In contrast, vacuum-cured MWCNT-free samples surpassed 45 MPa, indicating that curing protocols can significantly influence densification and mechanical properties. These findings underscore the trade-offs between material composition, curing approaches, and thermal stability, offering key insights into designing robust, resource-efficient lunar construction.

Keywords: lunar regolith composite, carbon nanotubes, compressive strength, lunar temperature cycling, coefficient of thermal expansion

Graphical Abstract

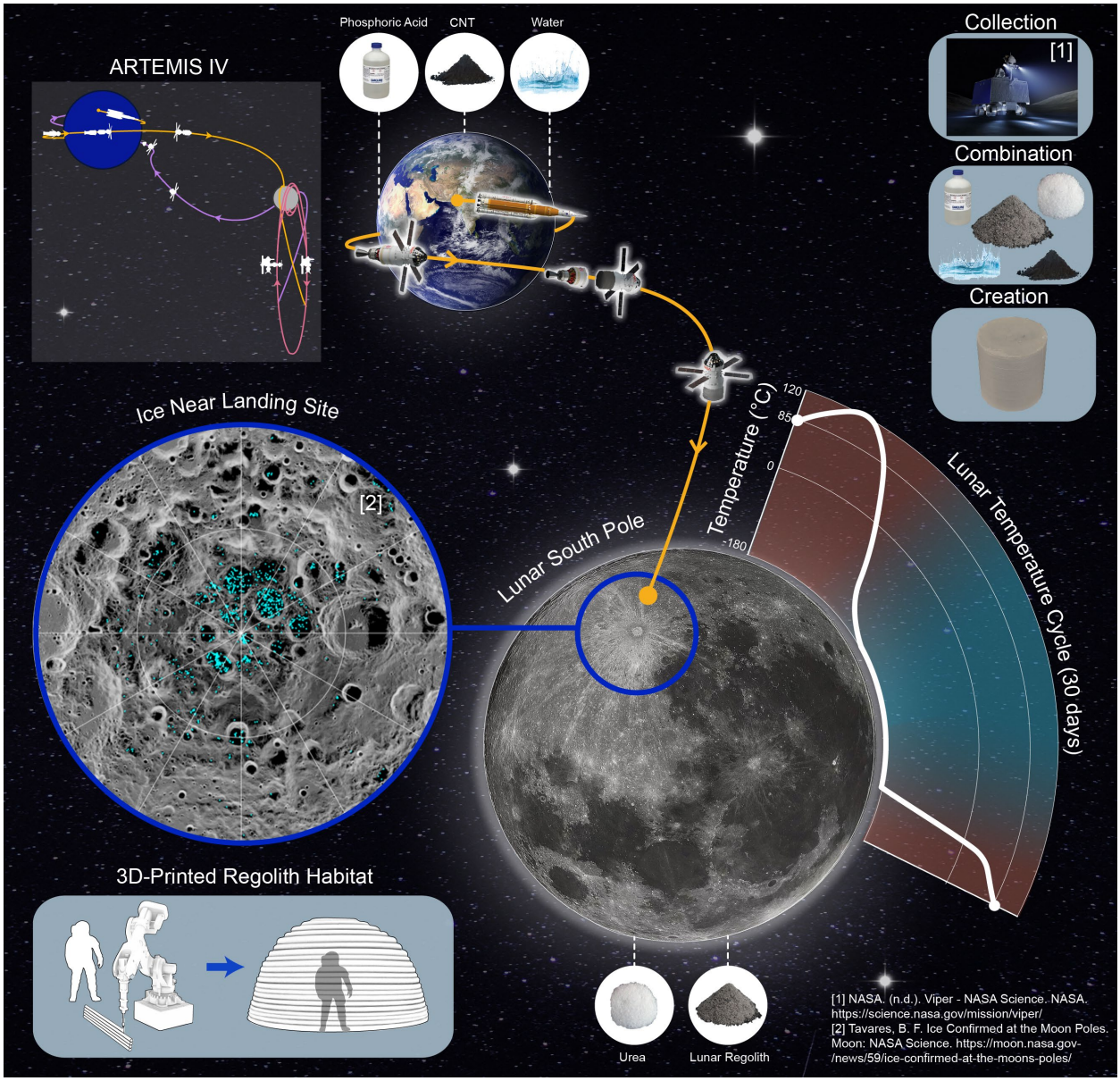

1. Introduction

Establishing sustainable habitats on the Moon or other celestial bodies requires overcoming numerous challenges, particularly in terms of resource management and material sourcing. Extraterrestrial construction faces significant resource constraints primarily due to the high cost of transporting materials. According to NASA, it costs around $10,000 to send one pound of material into orbit,[1] making sourcing local materials essential for lunar habitats. Due to this high cost, utilizing lunar regolith as a primary construction material becomes an important strategy as it can be excavated directly from the surface of the Moon. Additionally, the discovery of ice at the Moon's south pole further enhances the potential for in-situ resource utilization, as water serves multiple life-support[2] and various material applications. This has driven efforts to efficiently utilize limited water supplies, including combining regolith with acidic or alkaline solutions to create lunar concrete-like materials.[3] Another strategy to lower off-site material needs is to combine regolith with superplasticizers to lower water needs.[4] Urea, which serves as an effective superplasticizer, can be locally sourced from a human's urine, sweat, and tears.[5] Urea, disrupts hydrogen bonds, decreasing the viscosity of composite mixtures and improving their workability while minimizing water requirements. Similarly, attempts to 3D printing habitats using regolith mixtures[6] heavily depends on the workability of the materials used, as they must flow easily during the printing process while maintaining sufficient stability to form complex structures. Pilehvar et al.[7] found that the addition of urea in lunar regolith composites reduced the water needed for workability by up to 32%. However, researchers also found a direct relationship between increasing urea content and decreasing compressive strength under both vacuum and ambient pressure conditions. The results showed promise to decrease the water needs but to advance further, it is essential to develop materials that have a higher compressive strength.

Beyond the water usage, the harsh environmental condition on the Moon introduces additional engineering challenges, such as extreme temperature fluctuations ranging from -121 °C to 133 °C, radiation exposure, and micrometeorite impacts.[8] Thus, materials must withstand extreme temperature fluctuations and provide effective thermal insulation. A study by Zhang et al.[9] identified a 72-hour curing scheme as suitable for lunar pavement construction, with compressive strengths reaching 31.2 MPa. However, representative cycling tests caused

notable deterioration, including flexural strength reductions of up to 70%, microcrack formation, and increased porosity. These findings emphasize the importance of addressing not only vacuum conditions but also the repeated thermal stresses inherent to the lunar surface.

Identifying and implementing strategies to ensure mechanical properties while minimizing the detrimental effects of extreme environmental conditions is essential for space-based construction. In designing composites for space applications, there is often a balance between structural performance and payload mass. A compressive strength of approximately 6 MPa is typically adequate for lunar architecture due to lower gravity (one-sixth of Earth's),[10] but achieving higher strength, comparable to the 35 MPa needed for terrestrial structures,[11] is desirable to ensure safety in the extreme lunar condition. Existing literature reports lunar regolith composite compressive strengths ranging broadly from 12 MPa to 120 MPa, highlighting significant variability of additives and potential for further optimization.[12] Polymers, for instance, are unsuitable for space due to low thermal stability and, radiation sensitivity.[13] However, magnesium[14] is beneficial for sintering but is less practical for near-room-temperature curing conditions. CNTs on the other hand, offer significant advantages compared to other additives with their exceptional tensile/compressive strength, superior stiffness, enhanced structural integrity, and compatibility with 3D printing. CNTs have been widely used to augment various composite materials' mechanical properties and environmental resistance, such as aircraft components and concrete composites.[15-20] Bodnarova et al.[21] found that adding CNTs into concrete can effectively improve its mechanical properties and durability. Enhanced CNT dispersion improved mechanical properties by filling internal pores, reducing porosity, and strengthening the interface transition zone, resulting in greater compressive strength by 11.9 % and 17.30 % flexural strength, frost resistance, and impermeability, even after 100 freeze-thaw cycles. Since this study uses a very low concentration of CNTs (0.0015 wt% and 0.012 wt%), the impact on the matrix's overall thermal expansion properties is minimal, avoiding significant internal stresses during temperature changes. Several studies have highlighted the advantages of using CNTs in space applications due to their exceptional strength-to-weight ratio.[22] Notably, Garcia et al.[23] fabricated highly dense lunar regolith composites by applying 250 MPa of pressure in a pellet die and using CNT additives. The resulting compression properties enhanced from around 15 MPa using 0.60 wt% CNT to 100 MPa using 7.00 wt% CNT. However, since this study did not include lunar cycle temperature cycling, which is crucial for space habitation,

the true impact of CNT additives under these conditions remains uncertain. It is also anticipated that applying a pressure of 250 MPa, similar to that used by Garcia et al., would result in a significant increase in the strength observed in this study which only uses a pressure of 8 MPa due to equipment limitations. Despite the potential benefits, such high pressures are highly unfeasible for space applications.

Although prior research has demonstrated impressive compressive strengths using advanced matrices, many of these approaches rely on high water content (up to 30 wt%),[24] overlook temperature cycling tests,[25,26] or provide limited chemical analysis which are factors that limit their feasibility for lunar construction.[27] To address these gaps, the present study introduces a novel synthesis method that provides a more sustainable and efficient approach for constructing future lunar habitats. This method integrates MWCNTs into lunar regolith composites while minimizing water usage to 12.48 wt%. Additionally, it employs a particle size tuning strategy that combines an 80:20 ratio of fine-to-coarse regolith fractions to optimize the microstructure. MWCNTs are also paired with urea, and the research uniquely adopts an acidic formulation. Central to this study is its emphasis on the lunar environment, where stability is assessed through the effects of thermal cycling, vacuum pressure curing, and varying MWCNT weight percentages. By examining these factors' influence on microstructure and compressive strength, the study aims to develop regolith-based composites capable of achieving compressive strengths exceeding 35 MPa while retaining resilience under extreme lunar conditions. This work provides a comprehensive chemical, experimental, and simulation-based analysis of the benefits of CNTs for regolith composites, while also identifying areas for improvement. The proposed mechanisms offer valuable insights to guide future research directions and advance the development of optimized regolith-based materials for lunar habitats.

2. Results and Discussion

2.1 Mechanical Strength Enhancement with MWCNT Inclusion without Temperature Cycling

For the purpose of examining the lunar conditions' influence on the regolith composites, this study follows three distinct processing routes that are evaluated with different pre-conditions **(Figure 1a)**. Route 1 serves as the baseline for comparison consisting of ambient curing without temperature cycling. Route 2 combines ambient curing with four temperature cycles simulating extreme day-night fluctuations on the lunar surface **(Figure 1b)**. The temperature gradually

increases from 80 °C to a peak of 177 °C, then decreases to a minimum of -80 °C before returning to 80 °C, completing one full cycle. Route 3 starts with vacuum curing, followed by the same thermal cycling as in Route 2, thereby enabling an evaluation of how reduced atmospheric pressure and extreme temperature variations jointly influence composite performance. Unlike the Moon's continuous thermal gradient, we cycled between an oven, refrigerator, and ultra-freezer, which may have caused inconsistencies in thermal exposure. Real lunar temperatures lower to -121°C, but due to equipment limits, we only were able to reach -80°C.

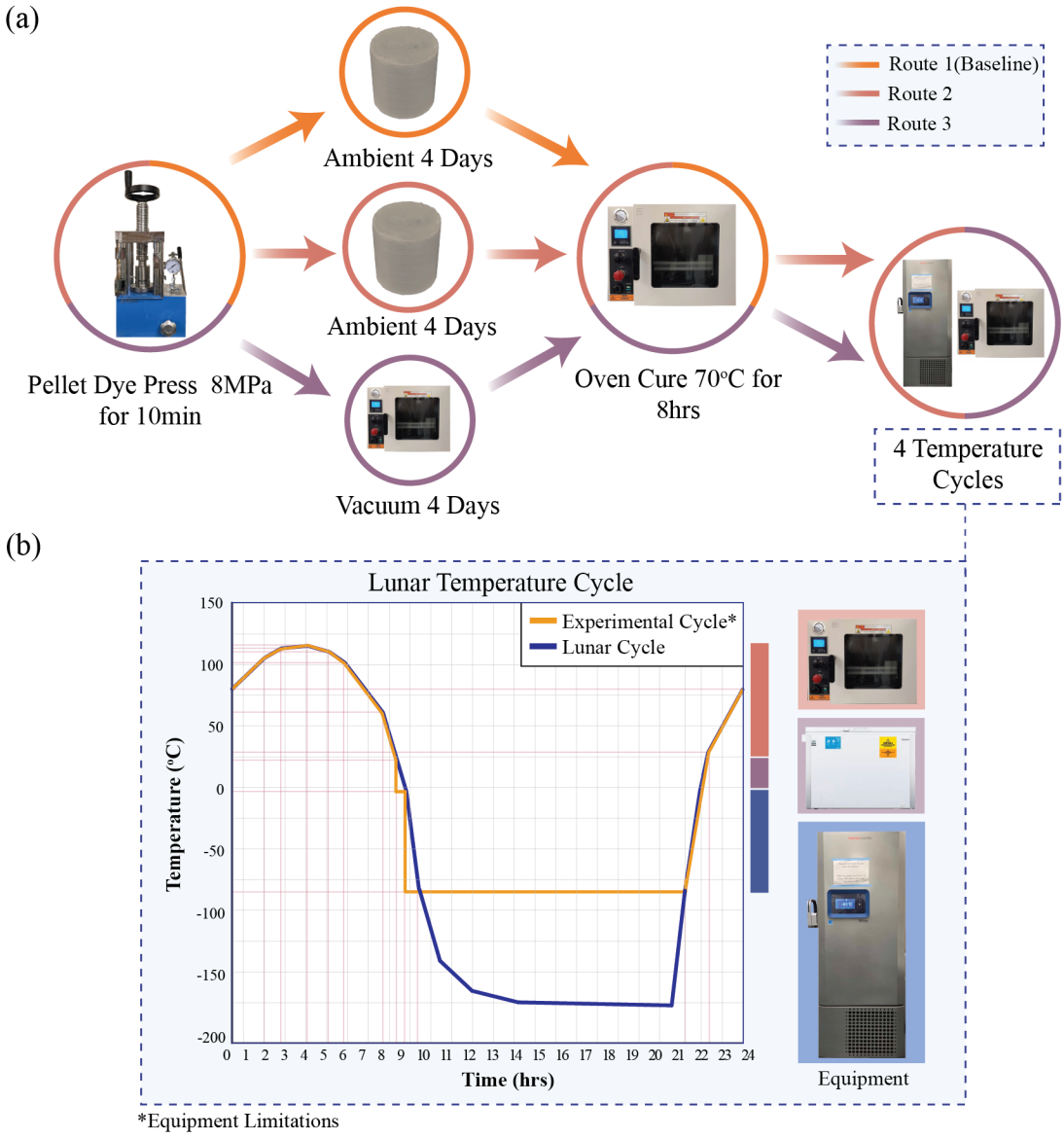

Figure 1. (a) Schematic illustration of the three curing routes for lunar regolith composites (b) Comparison of the experimental temperature cycle with the simulated lunar cycle.

In exploring the different processing routes with varying MWCNT concentrations, there is a focus on a more accessible processing approach using room temperature pre-curing conditions and low curing conditions (around 100 °C), in contrast to the high-temperature sintering processes (>1000) processes typically used in existing research.[28-30] The composition of the composite is illustrated in **Figure 2a**. A key aspect of the processing is the regolith method of mixing fine (<0.25 μm) and coarser (0.25 μm–250 μm) regolith particles **(Figure 2b)**. Based on preliminary experiments, the smaller particles filled voids between larger particles, effectively reducing porosity and directly contributing to improved compressive strength by creating a denser packing structure. The larger particles, on the other hand, mitigated shrinkage and cracking during curing by acting as a skeleton to counteract the stresses induced during the drying process. This optimizes particle size distribution, minimizes voids, increases packing density, reduces binder requirements, and enhances strength, impermeability, and volume stability.[31, 32] Leveraging natural particle gradation, this scalable approach represents a novel finding in regolith research.

Beyond the particle size optimization, this research further integrates urea and MWCNTs to reduce water requirements while enhancing the strength of lunar regolith composites **(Figure 2c)**. Unlike prior studies focusing on urea[33] or CNTs[34] individually, this approach leverages their synergistic effects. Urea acts as a superplasticizer reducing water content to 12.48 wt%, lower than typical lunar concrete formulations (5–30 wt%).[23,24] While urea reduces water usage, it causes a trade-off with strength, which was offset by adding MWCNTs to enhance compressive properties. Additionally, an acidic solution with phosphoric acid (H_3PO_4) was chosen as the pH modifier over the more commonly used sodium hydroxide due to its milder reactivity **(Figure 2d)**. Phosphoric acid contributes hydrogen donor molecules that form strong chemical bonds with regolith compounds, stabilizing the composite structure.[35] While sodium hydroxide's high pH facilitates the breakdown of silicates and metal oxides to form sodium silicate, phosphoric acid exhibits milder reactivity, dissolving some minerals and forming phosphate salts without overly aggressive reactions. Its stability, particularly at low temperatures, ensures long-term durability and resistance to extreme lunar temperature fluctuations.

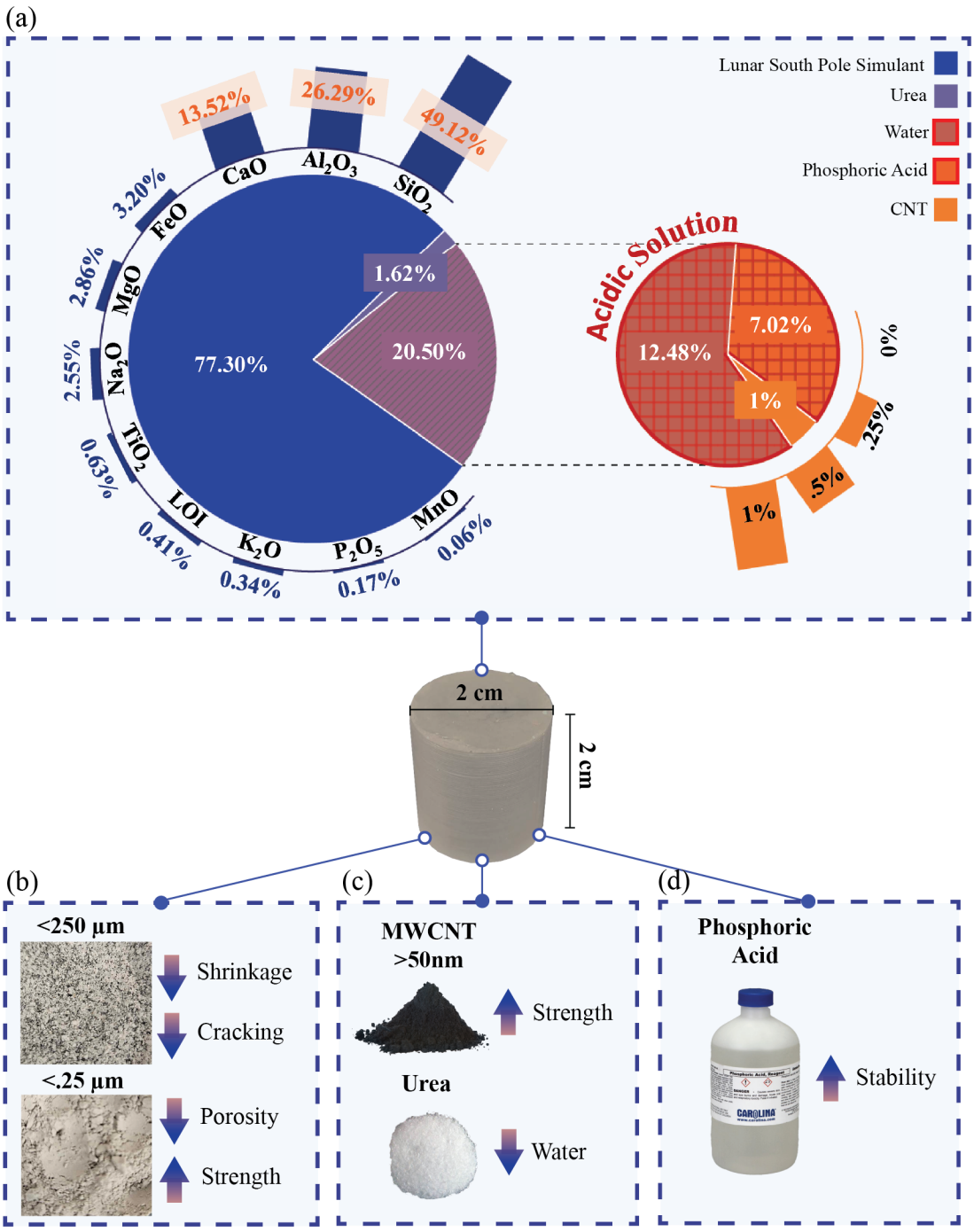

Figure 2. (a) Chemical composition of the composite (b) particle size tuning strategy (c) integration of urea and CNT (d) utilization of phosphoric acid as an acidic solution.

In order to validate the material modification and particle size optimization, the compressive strength, compressive modulus, and chemical characteristics of lunar regolith composites were

evaluated under ambient curing conditions without thermal cycling (Route 1), as illustrated in **Figure 3**. These experiments establish a baseline understanding of the effects of MWCNT incorporation on the compressive performance of composites. The compressive strength **(Figure 3a)** and compressive modulus **(Figure 3b)** results for Route 1 demonstrated a clear enhancement with the inclusion of MWCNTs. The sample with 0.50 wt% MWCNT exhibited the highest compressive strength, achieving 39 MPa (44.44% increase), and a compressive modulus of 1.98 GPa (41.43% increase) compared to the 27 MPa compressive strength and 1.4 GPa compressive modulus of the 0.00 wt% MWCNT sample. Additionally, the sample with 0.25 wt% MWCNT showed a marked increase in compressive strength with 31 MPa (14.81% increase) and 1.8 GPa compressive modulus, indicating the effectiveness of MWCNTs additives in reinforcing the composite in comparison with the MWCNT-free sample. However, when the MWCNT content was increased to 1.00 wt%, a slight decrease of compressive strength of 38 MPa and compressive modulus of 1.5 GPa was observed, compared to 39 MPa compressive strength and 1.98 GPa compressive modulus related to 0.50 wt% MWCNT specimen. This slight decrease indicates poor interfacial bonding between the CNTs and the matrix material.[36] When an excessive amount of CNTs disrupts the balance of distribution between CNTs and regolith particles, it negatively impacts and weakens the interfacial bonding between them, ultimately resulting in a decline in compressive strength.

To understand the compressive strength improvement achieved by incorporating MWCNTs into the composite under the ambient temperature curing method, an XRD technique was used as illustrated in **Figure 3c**. The characteristic peaks of MWCNTs observed at 23° and 30° correspond to graphite diffraction,[37] confirming that the hexagonal graphite structure of the MWCNTs remains intact across all samples.[38] The broad nature of these peaks at 23° and 30° reflects the layered arrangement of graphitic planes within the MWCNTs, highlighting the absence of significant long-range crystalline order. When 1.00 wt% MWCNT is incorporated into the composite, the XRD patterns reveal a noticeable increase in the intensity of the peaks at 23° and 30° compared to the 0.00 wt% MWCNT sample. This enhancement suggests that the MWCNTs influence the microstructure of the lunar matrix by improving packing density and promoting structural alignment, due to their high surface area and ability to act as nucleation sites during the curing process. In contrast, the 0.00 wt% MWCNT sample exhibits broader and lower-intensity peaks in the same region (23°, 30°), indicative of a less ordered and

predominantly amorphous structure, which may be due to the absence of the reinforcing effects provided by the MWCNTs. The results show that the sharper, higher-intensity peaks observed at 23° and 30° in the XRD patterns correlate with improved compressive strength, indicating that the presence of MWCNTs enhances the composite's structural order and compressive performance under the ambient curing method.

Beyond the microstructural alignment revealed by XRD, the chemical interactions between MWCNTs and the lunar matrix were examined using Fourier-Transform Infrared Spectroscopy (FTIR) **(Figure 3d)**. This analysis highlights the bonding mechanisms and changes in the chemical environment induced by MWCNT integration, further explaining their dual role in reinforcing and modifying the matrix network. The FTIR spectra reveals that incorporating MWCNTs into cementitious composites enhances the out-of-plane flexibility of silica tetrahedra, which can improve the material's adaptability, mechanical performance, and overall durability. This is evidenced by the sharper peak observed around 500 cm^{-1} in the MWCNT-containing sample, indicating a structural modification that increases the mobility of silica tetrahedra. Additionally, the reduced intensity observed in samples containing MWCNTs, compared to the 0.00 wt% MWCNT sample, suggests that MWCNTs help mitigate carbonation within the composite material. Carbonation, a chemical reaction between carbon dioxide and cement components, can degrade the material's structure over time, and the presence of MWCNTs appears to inhibit this process, enhancing the composite's durability. The presence of MWCNTs seems to interfere with this process, likely by altering the chemical environment, making it harder for carbonation to occur.[39] Peaks corresponding to specific functional groups further elucidate the nature of these interactions and their impact on the composite properties. In the 1700 cm^{-1} wavelength, associated with C=O stretching,[40] slight changes in intensity suggest that the MWCNTs interact with carbonyl-containing groups through secondary bonding mechanisms, such as hydrogen bonding, given their conjugated structure. These interactions improve the matrix cohesion by facilitating additional bonding sites, which enhance load transfer and stability under compressive loading condition. Furthermore, notable changes in the Si-O and Si-O-Si peaks (1000–500 cm^{-1})[41] highlight the influence of MWCNTs on the siloxane network, due to physical and chemical interactions that disrupt the original network while facilitating new interfacial bonds which enhance the structural integrity. MWCNTs not only act as reinforcing agents but also alter the chemical environment of the matrix, as evidenced by reduced

transmittance and variations in peak intensities, highlighting their dual role in disrupting and enhancing the matrix network through both chemical and physical mechanisms. These chemical modifications align closely with the observed improvements in mechanical properties, such as the compressive strength and modulus achieved with MWCNT incorporation. The enhanced bonding and structural alignment facilitated by MWCNTs provide a more robust matrix capable of withstanding greater mechanical loads, as evidenced by the 44.44% increase in compressive strength and 41.43% increase in modulus for samples containing 0.50 wt% MWCNTs. This synergy between chemical and mechanical enhancements underscores the effectiveness of MWCNTs in reinforcing the lunar regolith composite.

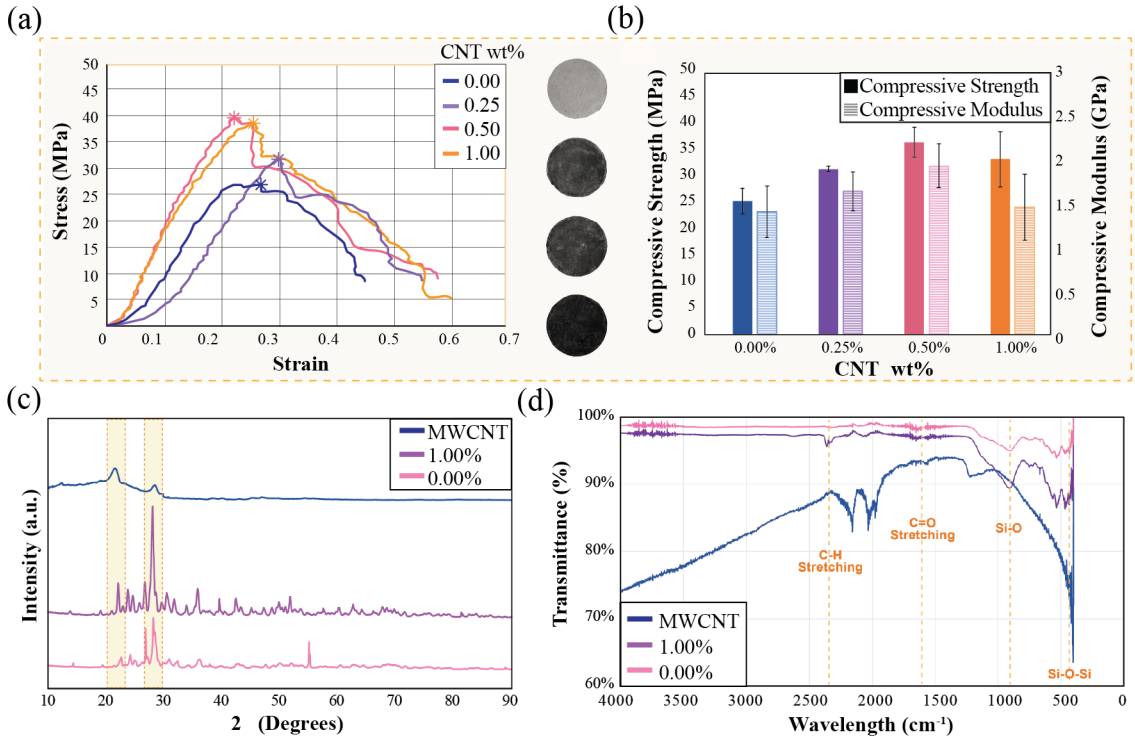

Figure 3. (a) Compressive strength and (b) modulus for ambient-cured composites (Route 1) (c) XRD spectroscopy for pure MWCNT, 0.00 wt%, and 1.00 wt% MWCNT composites fabricated under Route 1 (d) FTIR spectra for pure MWCNT, 0.00 wt%, and 1.00 wt% MWCNT composites fabricated under Route 1.

2.3 Thermal Cycling Effects on Compressive Properties

To ensure the suitability of lunar regolith composites for space applications, subjecting them to simulated lunar environments is crucial. Thermal cycling, which mimics the extreme

temperature fluctuations on the Moon, plays a crucial role in assessing material reliability. The results from mechanical testing demonstrated significant differences between the ambient-cured samples (Route 1) and those subjected to thermal cycling (Routes 2 and 3). While ambient-cured samples exhibited predictable trends in compressive strength and modulus with varying MWCNT concentrations, thermal cycling introduced inconsistencies and revealed critical challenges associated with composite behavior under lunar-like conditions.

In Route 2, which involved thermal cycling after ambient pre-curing, the compressive strength **(Figure 4a)** and modulus **(Figure 4b)** were inconsistent and showed no clear correlation with MWCNT content. While the 1.00 wt% MWCNT sample achieved the highest compressive strength (24 MPa) and modulus (1 GPa), the overall performance of Route 2 samples was significantly lower than Route 1, with all samples falling below 20 MPa. For example, the 0.00 wt% MWCNT sample in Route 2, despite its stability, achieved a compressive strength around 18 MPa with a compressive modulus of 0.98 GPa, falling short of the recorded 27 MPa compressive strength and 1.40 GPa compressive modulus of the 0.00 wt% MWCNT sample in Route 1. In contrast, Route 3 which combined vacuum pre-curing with thermal cycling, demonstrated better mechanical performance, with the 0.00 wt% MWCNT sample achieving a compressive strength of 47 MPa **(Figure 4c)** and modulus of 1.67 GPa **(Figure 4d)**. This improvement is unique, as vacuum pressure typically has a detrimental effect on compressive strength.[42] However, higher MWCNT content samples in Route 3 performed poorly, with the 1.00 wt% MWCNT sample showing a compressive strength of only 28 MPa and modulus of 1.36 GPa. This trend suggests that the thermal cycling process interacts with fabrication conditions and MWCNT wt% to significantly alter mechanical behavior compared to Route 1.

The inconsistencies in compressive strength and modulus between Routes 1, 2, and 3 can be explained by the role of water retention during fabrication. In Route 2, samples experienced significant water loss during the ambient exposure phase, leaving lower MWCNT wt% samples with approximately 50% water retention, while higher MWCNT wt% samples retained less than 20% **(Figure 4e)**. Excessive dryness in these levels of MWCNT wt% samples contributed to brittleness and poor mechanical performance. Route 3 on the other hand, i.e. Vacuum pre-curing retains higher water content by creating a localized humid environment that slows moisture loss. The absence of airflow reduces convective drying, while redistributed moisture remains trapped

within the material's microstructure. As a result, significant evaporation occurs predominantly during thermal cycling when heat drives moisture out more effectively **(Figure 4f)**. This controlled evaporation process promoted densification and reduced porosity in low MWCNT content samples, resulting in optimal water retention of around 35%, which correlated with superior compressive strength compared to Route 1 and Route 2, respectively. However, higher MWCNT content in Route 3 samples retained approximately 50% water after thermal cycling, leading to increased porosity and weaker interfacial bonding, which negatively impacted their strength. Under vacuum, the CNT network likely trapped water by limiting its escape pathways, creating localized moisture pockets. Additionally, the prevention of rapid surface evaporation in a vacuum, allows the CNT network to retain more water than ambient conditions.

While water retention plays a critical role in determining microstructural integrity, the significant reduction in compressive strength during thermal cycling, particularly in high MWCNT content samples, is largely attributed to the mismatch in thermal expansion coefficients (CTE) between the regolith matrix and MWCNTs (**Figure 5a**). MWCNT exhibited a negative CTE of $-1.2 \times 10-5/\ °C^{-1}$,[43] MWCNT shrinks when heated, whereas the regolith components, such as SiO_2 ($0.24 \times 10^{-6}/\ °C^{-1}$),[44] Al_2O_3 ($8.1 \times 10^{-6}/\ °C^{-1}$),[45] and CaO ($13.57 \times 10^{-6}/\ °C^{-1}$)[46] expand under the same conditions. This opposing thermal behavior generates significant internal stresses at the CNT-matrix interfaces during temperature fluctuations. These stresses disrupt the structural cohesion of the composite, leading to localized microcracking and delamination, which are more pronounced in samples with higher MWCNT concentrations. Consequently, while vacuum pre-curing improves strength by promoting densification, the addition of MWCNTs aggravates the thermal mismatch issue, reducing mechanical performance during cycling.

To further investigate and quantify the effects of CTE mismatch, thermal cycling simulations were conducted to model the stress and strain distributions in MWCNT-reinforced composites under lunar-like temperature fluctuations. The simulations utilized a representative volume element (RVE) approach, with the RVE extracted from a larger computational model populated with homogeneously distributed, randomly oriented MWCNTs (**Figure 5b**). The MWCNTs were modeled as solid cylinders with diameters of 20 nm and lengths between 1-15 μm, ensuring no intersections or overlaps to replicate a realistic microstructure. The chosen RVE size of $5 \times 5 \times 5$ μm^3 included a MWCNT volume fraction of 0.77%, closely matching the experimental value of

0.71% (equivalent to 0.5 wt%). The finite element model, implemented in general finite element analysis software, ABAQUS, with a coupled temperature-displacement solver, applied a heating-cooling-heating cycle ranging from 80 °C to 117 °C, cooling to -80 °C, and returning to 80 °C. This setup simulated the thermo-mechanical interactions arising from differences in the CTEs of the MWCNTs and the matrix material.

The results of the thermal cycling simulations revealed significant tensile stress concentrations at the maximum temperature of 117 °C, particularly around the MWCNTs and along their axial directions (**Figure 6**). These stress concentrations arose from the higher stiffness of the MWCNTs and their mismatched thermal expansion properties relative to the regolith matrix. This behavior indicates that MWCNTs act as stress concentrators, amplifying the effects of thermal mismatch within the composite. The strain distributions further highlighted this phenomenon, showing elevated tensile strains in the regions surrounding the MWCNTs, consistent with the localized stress concentrations. After the thermal cycling finished, at 80 °C, the stress distributions partially normalized. However, residual stresses and strains persisted near the MWCNT-matrix interfaces reflecting the thermal expansion mismatch accumulated during the heating and cooling cycle. The strain contours at this stage showed localized deformation patterns near the MWCNTs, underscoring the lasting mechanical constraints imposed by the MWCNT reinforcement. These residual stresses and localized strains contribute to the long-term weakening of the composite structure. The alternating compressive and tensile stresses throughout the thermal cycle amplify these effects increasing the likelihood of microcracking and delamination, particularly in composites with high MWCNT content.

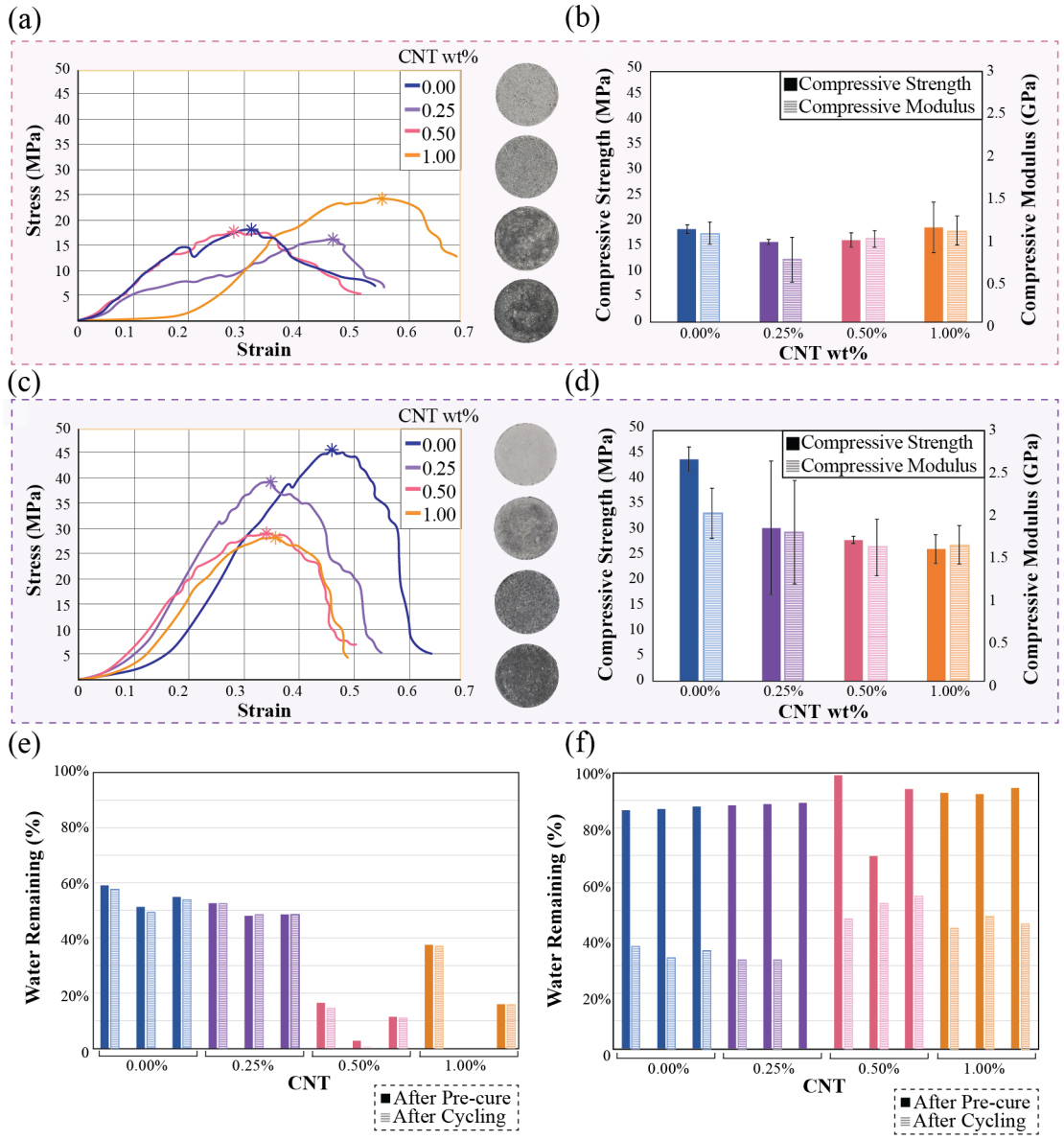

Figure 4. (a)-(d) Compressive strength and compressive modulus of ambient cured (Route 2) and vacuum cured (Route 3) specimens with temperature cycling, respectively (e)–(f) remaining water content after pre-curing and post-cycling for samples fabricated under Routes 2 and 3, respectively.

(a)

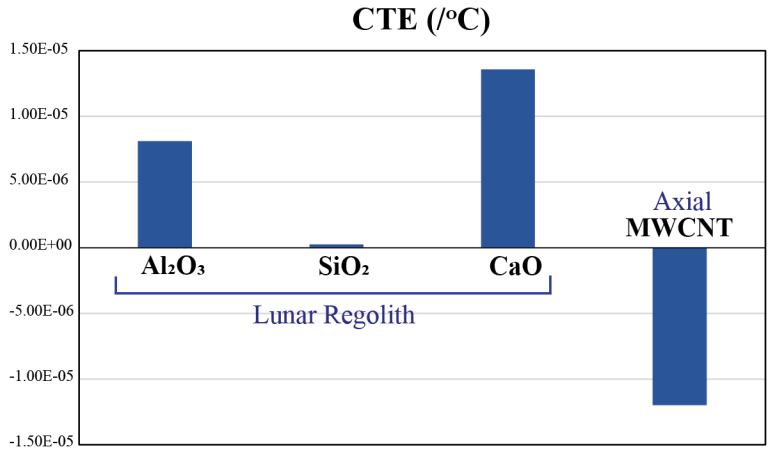

(b)

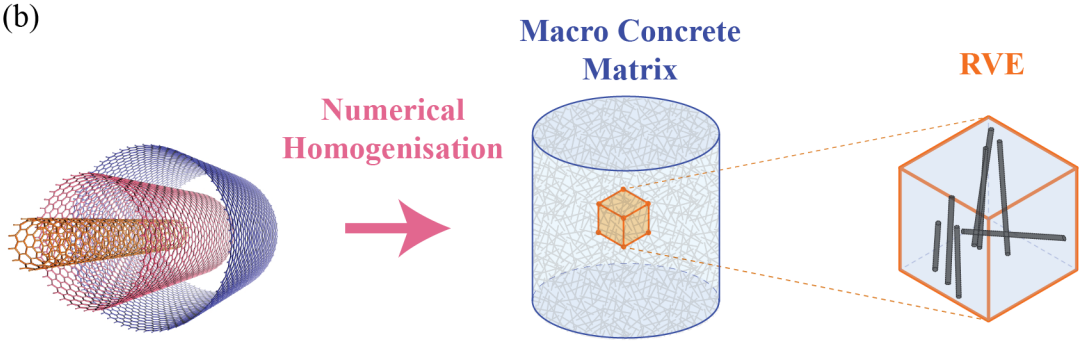

Figure 5. (a) Coefficients of thermal expansion for the three main lunar regolith components (Al_2O_3, SiO_2, CaO) and axial MWCNT (b) schematic of the RVE modeling approach incorporating MWCNT distribution.

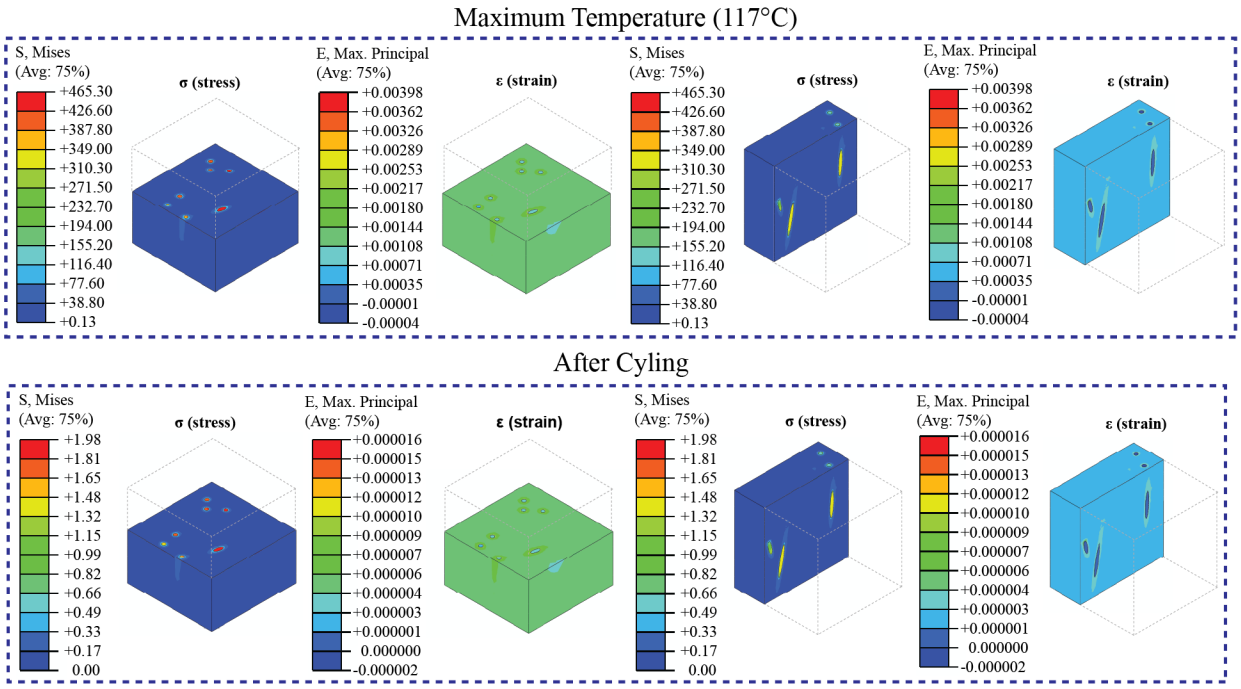

Figure 6. Stress and strain distribution resulted from simulation along the x and y sections at the peak temperature of 117 °C and after one complete temperature cycle in an representative volume element of the lunar regolith composites containing MWCNTs.

2.4 Comparative Evaluation of MWCNT-Incorporated Composites

Achieving consistent compressive strength in composites relies heavily on uniform particle dispersion. To evaluate the quality of dispersion, Scanning Electron Microscopy (SEM) and Energy Dispersive Spectroscopy (EDS) are employed to visualize and analyze the distribution of materials within the composite with 1.00 wt% MWCNT across the three processing routes (**Figure 7**). The SEM images for all samples across the three synthesis routes reveal minimal porosity, a crucial characteristic for enhancing material strength. The microstructure includes a mix of small and large particles, reflecting a deliberate particle-size blending strategy designed to optimize packing density and mechanical properties. However, the significant differences in the distribution of MWCNTs are visible among different routes, providing insight into their reinforcement efficiency under different fabrication conditions. In the Route 1 samples (ambient curing without temperature cycling), the MWCNTs appear to wrap around the regolith particles, creating a smoother overall morphology **(Figure 7a)**. This wrapping behavior enhances

interfacial bonding and contributes to improved load transfer within the composite, as evidenced by the smoother textures in the corresponding SEM images (detailed further in **Figure S1** in the Supporting Information). The smoother morphology aligns with the minimal thermal stresses present in Route 1, as these samples were not subjected to temperature cycling. The uniformity of the matrix and the close interaction between MWCNTs and particles provide evidence of a cohesive composite structure, reinforcing the mechanical stability, as illustrated in **Figure 3a**. Conversely, the temperature-cycled samples (Route 2 and Route 3) display a distinct separation between the MWCNTs and the regolith particles, resulting in a rougher morphology **(Figure 7b, 7c)** (detailed further in **Figure S2 and Figure S3** in the Supporting Information). The separation in the regolith-MWCNT composite after temperature cycling arises from the mismatch in their coefficients of thermal expansion (CTE). This discrepancy causes stress at the interface, leading to delamination and affecting the composite's structural integrity. This separation was more pronounced in the vacuum-cured Route 3 samples, suggesting that thermal cycling introduces the CTE mismatch between the MWCNTs and the regolith matrix. To ensure that the observed MWCNT distribution was not affected by the presence of urea, EDS mapping was conducted on a control sample without urea (**Figure 7d**) and a standard sample containing urea (**Figure 7e**). Since urea introduces additional carbon into the matrix, this comparative analysis was essential to isolate the contribution of MWCNTs. The results demonstrate a homogeneous distribution of MWCNTs in both cases, confirming that the addition of urea did not adversely affect dispersion. This uniform dispersion, achieved by directly dispersing MWCNTs into the acidic solution, effectively prevented MWCNT conglomeration, which is critical for avoiding stress concentrations and maintaining composite integrity. However, the SEM images indicate that the primary issue lies not in MWCNT dispersion, but in the weakened interfacial adhesion caused by temperature cycling. While the uniform distribution of MWCNTs should theoretically enhance load transfer and mechanical performance, the separation between MWCNTs and regolith particles observed in cycled samples undermines this potential. The rougher texture corresponds to reduced interfacial bonding, with MWCNTs failing to form an interconnected network with the surrounding particles. This weak adhesion likely limits the efficiency of load transfer and contributes to stress concentrations at the interfaces between the MWCNT and regolith particles, particularly under temperature cycling conditions. In addition to the adhesion challenges, the separation observed in temperature-cycled samples highlights the role of CTE mismatch. The

contrasting CTEs of the MWCNTs (negative) and the regolith matrix (positive) introduce internal stresses during heating and cooling cycles further degrading the composite structure. These stresses amplify microcracking risks, particularly in high MWCNT content samples where the MWCNT concentration intensifies these effects. Therefore, while the fabrication process ensures uniform MWCNT dispersion, thermal cycling disrupts interfacial adhesion and matrix cohesion, ultimately reducing the compressive strength of the composite.

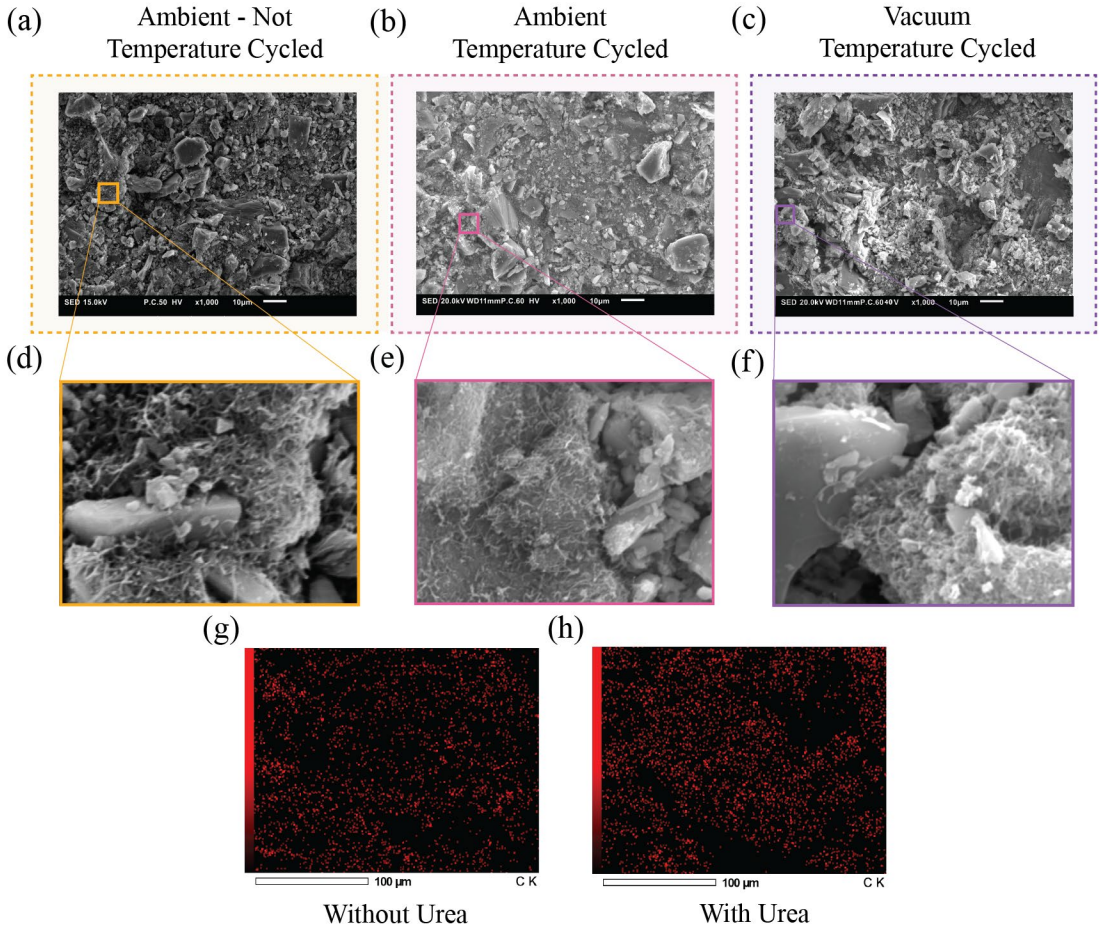

Figure 7. (a)-(c) SEM images of 1.00 wt% MWCNT samples with callouts (d)-(f) highlighting visible MWCNTs fabricated under ambient-cured, non-cycled condition (Route 1), ambient-cured with temperature cycling condition (Route 2), and vacuum-cured with temperature cycling condition (Route 3), respectively, (g) EDS image showing carbon distribution in the control

sample without urea (h) EDS image showing carbon distribution in the Route 1 sample with urea.

The uniformity of both particle dispersion and degree of dryness is crucial for maintaining a well-supported composite structure, as evaluated in the SEM and EDS analyses. Both forms of analyses supported that MWCNTs had uniformly dispersed throughout all routes with a good mixing strategy, avoiding conglomerations that weaken the composite. However, the SEM images further demonstrated that temperature cycling (Routes 2 and 3) introduced interfacial adhesion challenges due to the separation of MWCNTs and regolith particles, which intensified the internal stress gradients generated during the curing process. These findings correlate directly with the failure patterns observed in the compressive tests, as illustrated in **Figure 8**.

Following the compressive tests, failure in the samples consistently began with exterior damage, leading to slight hourglass-shaped deformation on the interior parts **(Figure 8a)**. These failure patterns were observed across all samples fabricated via different processing methods including ambient curing with no cycling **(Figure 8b)**, ambient curing with cycling **(Figure 8c)**, and vacuum curing with cycling **(Figure 8d)**. This suggests that the exterior parts of the sample cure more efficiently than the interior parts. Cylindrical samples are prone to fracture at any point along the sides or edges, with fractures occurring both in the middle and at the outer parts of the specimens.[47] This failure, referred to as 'hourglass failure', happens when the load is applied uniformly at the center, resulting in symmetrical failure across all sides due to the absence of loading eccentricity.[48] Although the pattern of breakage was consistent across all routes, slight differences were observed in the breakage process. Routes 1 and 3 exhibited more visible cracks and breakage, while Route 2 retained its shape without significant break-off damage. This suggests that the high compressive strength observed in Routes 1 and 3 is primarily due to their hard exterior, even though the interior was not fully dried. In contrast, Route 2 demonstrated lower performance with compressive strengths falling below 20 MPa. This indicates that the outer layer, which is the first to break off, was not as hard in Route 2 compared to the other routes, as evidenced by the lack of pronounced breakage.

The uneven drying process during curing plays a critical role in creating internal stress gradients, which weakens the composite structure. As the material cures, moisture migrates from the interior to the exterior, causing the outer layers to dry faster. This differential drying leads to

greater shrinkage on the exterior, generating tensile stresses that can initiate failure on the outer layers. Although the interior is weaker due to these internal stress gradients, the exterior typically experiences higher surface tension during drying, further contributing to localized damage and structural weakening. These stress gradients are less pronounced in Route 1 due to the absence of temperature cycling, resulting in smoother and more cohesive fracture surfaces. In contrast, temperature cycling in Routes 2 and 3 intensified the internal stresses, leading to brittle failure and rougher fracture surfaces due to weakened interfacial adhesion and separation between MWCNTs and regolith particles.

Building on the microstructure characteristics of samples fabricated through different routes, the toughness data provides a comparative measure of the material energy absorption under compressive load **(Figure 8e)**. In Route 1, the toughness increased significantly from 0.64 MPa for 0.00 wt% specimen to 1.17 MPa for 0.5 wt% with increasing the MWCNT wt%, however, a slight decrease to 1.06 MPa was observed at 1.00 wt% MWCNT content. This increasing trend is attributed to the enhanced strength and ductility imparted by MWCNT reinforcement. This improves the material's capacity to resist deformation and failure under compressive forces. However, the decline at 1.00 wt% MWCNT is due to poor interfacial bonding, which compromises structural integrity. In contrast, Route 2 exhibits no clear or consistent trend in toughness with results ranging from 0.40 MPa to 0.60 MPa. The lack of a clear pattern suggests that temperature cycling disrupted the interaction between MWCNTs and the composite matrix, potentially due to thermal mismatch stresses or microstructural changes caused by repeated expansion and contraction. These inconsistencies highlight the challenges of maintaining uniform performance when the composite is subjected to thermal fluctuations. For Route 3, the toughness gradually decreases from 1.20 MPa to 0.76 MPa as MWCNT wt% increases from 0.00 wt% to 1.00 wt% respectively. While the vacuum curing process positively influences the overall curing quality and minimized porosity, the higher MWCNT concentrations are adversely affected by the temperature cycling. These results from the amplified CTE mismatch between the MWCNT and the regolith, lead to microcracks and reduced energy absorption capacity. The decreasing trend in Route 3 closely aligns with the observed compressive strength data and the separation of MWCNT and regolith particles observed in SEM images. This also emphasizes the interconnected roles of the MWCNT wt%, curing conditions, and mechanical properties.

The performance trends observed across the three fabrication routes highlight the critical influence of processing conditions on mechanical properties. To contextualize these results, the Ashby plot of compressive strength versus density highlights the performance of various material systems in comparison with this study **(Figure 8f)**.[49-52] This study occupies a unique position at the intersection of plastics, metals, composites, concrete, and ceramics. This unique placement underscores their versatility and suitability for a wide range of structural applications, offering an optimal balance of strength and lightweight properties tailored to diverse engineering demands. We demonstrated a promising synthesis process that achieved comparative performance. It is anticipated that utilizing higher pressure during the fabrication process would substantially enhance the strength. Nonetheless, applying low pressure (8 MPa) during our fabrication process is more practical and feasible for lunar construction due to the limitations of available equipment and the constraints of operating in the Moon's environment.

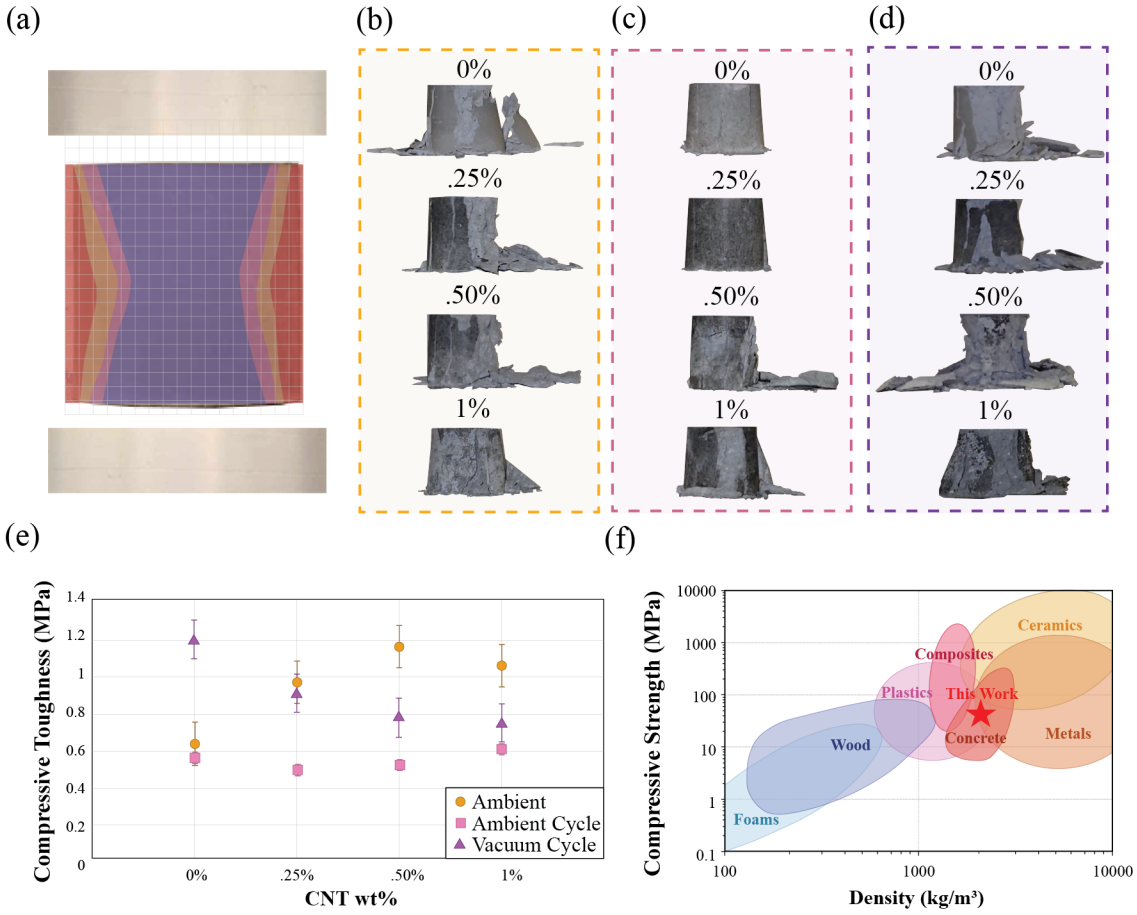

Figure 8. (a) Schematic illustrating failure patterns observed during compressive test (b)-(d) post-compression failure patterns for specimens with varying MWCNT wt% fabricated under ambient non-cycled, ambient-cycled, and vacuum-cycled routes, respectively (e) comparisons of compressive toughness of the specimens fabricated under three distinct routes. Visualization of compressed sample fabricated under (f) Ashby plot comparing compressive strength vs. density of this study against other literature.

3. Conclusion

This study presents a detailed exploration of the complex interplay between MWCNT reinforcement and lunar regolith composites under varied curing conditions, highlighting both the potential and limitations of using MWCNTs in extraterrestrial construction. The results of the different processing routes, including ambient cured with no cycling (Route 1), ambient cured with cycling (Route 2), and vacuum cured with cycling (Route 3), demonstrate that incorporating MWCNTs significantly enhances composite strength under specific conditions. In ambient curing without cycling, samples achieved a high compressive strength of 39 MPa at 0.50 wt% MWCNT, representing a 44.44% improvement over the 0.00 wt% MWCNT sample. However, thermal mismatch between the negative CTE of MWCNTs and the positive CTE of the regolith matrix limited durability during lunar temperature cycling, causing microcracking and reduced performance. Under vacuum curing and temperature cycling, the 0.00 wt% MWCNT composite achieved the highest strength of 47 MPa, attributed to enhanced densification from accelerated moisture evaporation and an optimal water retention level of 35%, while the 1.00 wt% MWCNT sample performed the worst at 28 MPa. Addressing thermal mismatch challenges requires optimizing CTE compatibility or developing tailored CNT variants to enhance compressive strength and durability under lunar conditions. This study highlights the importance of testing composites under realistic conditions and reveals that the MWCNTs used in this study are incompatible with the regolith matrix during temperature cycling. Improving CTE compatibility is key to mitigating thermal stresses and enhancing material durability for extraterrestrial construction.

4. Methods

4.1 Materials

The regolith used in this study is LSP-1 Lunar South Pole Simulant, sourced from Exolith Lab with a particle size range of <0.04 μm – 1000 μm. For the particle size strategy, larger particles were screened out using a sifter, while smaller particles were generated through grinding and further sieving (20×60 mesh). To reduce water requirements, urea granules with a 99.0–100.5% assay (anhydrous basis) are from Lab Alley and utilized as a superplasticizer. An acidic solution composed of water and 85% ACS-grade phosphoric acid is prepared, with the acid sourced from Oakwood Chemical. Multi-walled carbon nanotubes with a diameter greater than 50 nm and a length of 10-20 μm, purchased from Cheap Tubes Inc., are incorporated to investigate their effects on the mechanical compressive strength of the composite.

4.2 Fabrication

The composite system itself comprises five primary components: lunar regolith, urea, distilled water, phosphoric acid, and MWCNT powder (>50 nm), with approximately 77.36 wt% derived from a simulated South Pole regolith. An acidic solution of phosphoric acid mixed with distilled water constitutes about 19.50 wt% of the mixture. After the preparation of all the materials, they are thoroughly mixed manually for three minutes to form a homogeneous slurry. To ensure consistent testing, three replicates of each MWCNT loading were prepared and subjected to uniaxial compression at 8 MPa for ten minutes using a 20 mm diameter pellet die (Specac, USA). After compression, specimens proceeded through one of the three curing pathways. Route 1 involved ambient air curing for four days followed by eight hours at 70 °C in an oven. Route 2 followed the same ambient and oven curing but introduced four temperature cycles to simulate lunar day-night extremes, while Route 3 replaced ambient curing with four days in a vacuum chamber and then vacuum oven curing at 70 °C for eight hours, followed by the same thermal cycling. Temperature pre-conditioning was based on the lunar surface extremes reported by Malla et al.[53] which is approximately 114 °C during daytime to −171 °C at night. Due to equipment constraints, the minimum temperature in this study was adjusted to −80 °C, and the typical 14-day lunar cycle was compressed into 24 hours for practical implementation. Although this work used a maximum achievable vacuum of −0.1 MPa, future studies may aim for conditions nearing 3.04×10^{-15} atm[54] to more closely replicate the near-total vacuum on the Moon. Once curing and pre-conditioning were complete, all specimens underwent chemical analyses and mechanical testing to evaluate their performance under simulated lunar conditions.

4.3 Characterization

Chemical analysis is performed to confirm the composition quality of the samples and ensure uniform dispersion of the components in the composite samples. Residual water content was quantified to evaluate the impact of different curing routes on residual water content. For each MWCNT weight percentage under Routes 2 and 3, three samples were weighed before and after thermal curing, and after cycling. Additionally, the density was calculated at these three stages, both with and without assuming complete water evaporation. From these values, the accurate assumption of water remaining was calculated to determine the percentage of residual water content.

The bonding structures of the composites with no cycling are further analyzed using FTIR. FTIR spectroscopy is conducted with a Thermo Nicolet 6700 FT-IR spectrometer (Thermo Fisher Scientific) in transmittance mode over a wavenumber range of 4000–400 cm^{-1}, focusing on the bottom surface area of each sectioned sample. The crystallographic structures of the composites are analyzed using X-ray Diffraction (XRD). XRD measurements are performed using a Bruker D2 Phaser with LYKXEYE 1D silicon strip detector, employing Cu K$\propto$ radiation (λ = 1.5406 Å). Data are collected over a 2θ range of 10–90° at a scanning rate of 3°/min, with a step size of 0.05°. Powdered samples are prepared to ensure uniformity and minimize preferred orientation effects, allowing for accurate analysis of the composite's crystalline and amorphous phases. A batch of composites in all routes are sectioned vertically for SEM and EDS analysis. SEM is utilized to examine porosity and surface texture across the 1.00 wt% CNT concentration for the three curing routes and EDS is performed on the 1.00 wt% CNT sample to map the distribution of MWCNTs.

4.4 Mechanical Analysis

The compressive strength of the lunar regolith composites is evaluated using a Materials Test System (MTS) machine with 80 kN load cell. Compressive strength tests are conducted on samples containing 0 wt%, 0.25 wt%, 0.50 wt%, and 1.00 wt% CNTs, with a controlled displacement rate of 1 mm/min. From the compressive strength, the compressive modulus is calculated. Additionally, the toughness factor is determined by calculating the area under the stress-strain curve through numerical integration. The fracture behavior of each sample is

analyzed to provide further insight into the mechanical properties and failure mechanisms of the composites.

4.5 Computational Analysis

An in-depth analysis of the CTE is conducted to elucidate the underlying mechanisms driving the results. Notably, this represents the first such investigation for lunar regolith. A simulation basis is developed to investigate thermal mismatch and the resultant thermal stresses in MWCNT reinforced nanocomposite matrices based in lunar regolith. The computational approach is integrated with the experimental methodology to validate the behavior of MWCNTs within the composite under lunar temperature fluctuations. A model of the concrete matrix is then created, beginning with generating a larger domain populated with homogeneously distributed, and randomly oriented MWCNTs using a Python script. The MWCNTs were modeled as solid cylinders with a diameter of 20 nm and lengths ranging from 1-15 μm, distributed without intersections or overlaps to replicate a realistic microstructure. Subsequently, a smaller sub-domain rich in MWCNT density was extracted from the larger domain to serve as the three-dimensional RVE for thermal stress analysis. The chosen RVE size was $5 \times 5 \times 5$ μm³, with a fiber volume fraction of 0.77%, closely matching experimental samples (0.71%, equivalent to 0.5 wt%).

The finite element model for the selected RVE is implemented in Abaqus using a coupled temperature-displacement solver to analyze thermo-mechanical interactions. Both the MWCNTs and the lunar regolith matrix are modeled as linear elastic materials with isotropic coefficients of CTE to capture their thermal behavior **(Table S1)**. A temperature field is applied to all outer surfaces to simulate thermal effects, following a heating-cooling-heating cycle replicating one cycle used for this study: the temperature rises from 80 °C to 117 °C, cooled to -80 °C, and then returned to 80 °C. This cycle is designed to elucidate thermal mismatch effects arising from differences in the CTEs of the MWCNTs and the matrix material.

Boundary conditions of the temperature cycle and displacement are defined to ensure accurate simulation results. Since the sample rests on a surface, penetration is not possible. To account for this, one surface of the RVE is fixed to prevent rigid body motion, while the other surfaces are allowed to deform freely. The interface between the MWCNTs and the lunar regolith is modeled using a "Tie" contact with the nodes-to-surface option, ensuring accurate

representation of contact mechanics. A fine mesh with a size of 03 μm is used, employing linear 4-node thermally coupled tetrahedral elements. This meshing strategy achieves a balance between computational efficiency and the resolution required to capture significant thermal and mechanical stress gradients. Thermal stress evolution during the heating and cooling cycles is then analyzed to understand the impact of CTE mismatches between the MWCNTs and the matrix material. The residual stresses following the cycle provide insights into microstructural stress distributions and their potential effects on the mechanical integrity of the composite under cyclic thermal loading.

Supporting Information

Supporting Information is available from the Wiley Online Library or from the author.

Acknowledgments

The material is based upon work supported by NASA under award No 80NSSC24K1347. The author would also like to thank Seneca Ceramics for their assistance in grinding the regolith. The authors also thank many helpful discussions with Dr. Weiwei Zheng (Associate Professor of Chemistry at Syracuse University).

References

(1) Hammond, W. E. *Design methodologies for space transportation systems*; Aiaa, 2001.

(2) Ellery, A. Supplementing closed ecological life support systems with in-situ resources on the moon. *Life* **2021**, *11* (8), 770.

(3) Wang, Y.; Hao, L.; Li, Y.; Sun, Q.; Sun, M.; Huang, Y.; Li, Z.; Tang, D.; Wang, Y.; Xiao, L. In-situ utilization of regolith resource and future exploration of additive manufacturing for lunar/martian habitats: A review. *Applied Clay Science* **2022**, *229*, 106673.

(4) Aïtcin, P.-C. The use of superplasticizers in high performance concrete. In *High Performance Concrete*, CRC Press, 2018; pp 14-33.

(5) Roberts, A. D.; Whittall, D.; Breitling, R.; Takano, E.; Blaker, J. J.; Hay, S.; Scrutton, N. S. Blood, sweat, and tears: extraterrestrial regolith biocomposites with in vivo binders. *Materials Today Bio* **2021**, *12*, 100136.

(6) Korniejenko, K.; Pławecka, K.; Kozub, B. An overview for modern energy-efficient solutions for lunar and martian habitats made based on geopolymers composites and 3D printing technology. *Energies* **2022**, *15* (24), 9322.

(7) Pilehvar, S.; Arnhof, M.; Erichsen, A.; Valentini, L.; Kjøniksen, A. L. Investigation of severe lunar environmental conditions on the physical and mechanical properties of lunar regolith geopolymers. *journal of materials research and technology* **2021**, *11*, 1506-1516.

(8) *Caela, B.*; *Liam, M.* Weather on the Moon. NASA.

(9) Zhang, R.; Zhou, S.; Li, F. Preparation of geopolymer based on lunar regolith simulant at in-situ lunar temperature and its durability under lunar high and cryogenic temperature. *Construction and Building Materials* **2022**, *318*, 126033.

(10) Mathieu, M.; Haji Abdulrazagh, P.; Jablonski, A. M.; Maghoul, P. Topological Interlocking Bricks for Habitat Construction in Extraterrestrial Environments. In *Earth and Space 2024: Engineering for Extreme Environments*, 2024; pp 858-867.

(11) Association, N. R. M. C. CIP 35-testing compressive strength of concrete. *Concrete in Practice: What, Why and How* **2003**.

(12) Bao, C.; Zhang, D.; Wang, Q.; Cui, Y.; Feng, P. Lunar In Situ Large-Scale Construction: Quantitative Evaluation of Regolith Solidification Techniques. *Engineering* **2024**.

(13) Pastore, R.; Delfini, A.; Albano, M.; Vricella, A.; Marchetti, M.; Santoni, F.; Piergentili, F. Outgassing effect in polymeric composites exposed to space environment thermal-vacuum conditions. *Acta Astronautica* **2020**, *170*, 466-471.

(14) Osio-Norgaard, J.; Hayes, A. C.; Whiting, G. L. Sintering of 3D printable simulated lunar regolith magnesium oxychloride cements. *Acta Astronautica* **2021**, *183*, 227-232.

(15) Hoe, A. J.; Lin, W.; Wang, Y. A Compositional Study of Regolith Composites With Carbon Nanotube Additives for Extraterrestrial Construction. In ASME Aerospace Structures, Structural Dynamics, and Materials Conference, 2023; American Society of Mechanical Engineers: Vol. 87141, p V001T003A014.

(16) Ding, S.; Wang, X.; Qiu, L.; Ni, Y. Q.; Dong, X.; Cui, Y.; Ashour, A.; Han, B.; Ou, J. Self-sensing cementitious composites with hierarchical carbon fiber-carbon nanotube composite fillers for crack development monitoring of a maglev girder. *Small* **2023**, *19* (9), 2206258.

(17) Bheel, N.; Mohammed, B. S.; Woen, E. L. Modelling and optimizing the impact resistance of engineered cementitious composites with multiwalled carbon nanotubes using response surface methodology. *Scientific Reports* **2024**, *14* (1), 24107.

(18) Wu, Z.; Zhao, Y.; Yang, K.; Guan, J.; Wang, S.; Gu, Y.; Li, M.; Feng, Y.; Feng, W.; Ritchie, R. O. Enhancing the mechanical performance of fiber-reinforced polymer composites using carbon nanotubes as an effective nano-phase reinforcement. *Advanced materials interfaces* **2023**, *10* (3), 2201935.
(19) Jing, Y.; Lee, J. C.; Moon, W. C.; Ng, J. L.; Yew, M. K.; Jin, Y. Durability and environmental evaluation of rice husk ash sustainable concrete containing carbon nanotubes. *Scientific Reports* **2025**, *15* (1), 4352. DOI: 10.1038/s41598-025-88927-z.
(20) Chen, X.; Cheng, P.; Tang, Z.; Xu, X.; Gao, H.; Wang, G. Carbon-based composite phase change materials for thermal energy storage, transfer, and conversion. *Advanced Science* **2021**, *8* (9), 2001274.
(21) Bodnarova, L.; Jarolim, T. Study the effect of carbon nanoparticles in concrete. In *IOP Conference Series: Materials Science and Engineering*, 2018; IOP Publishing: Vol. 385, p 012006.
(22) Ramachandran, K.; Boopalan, V.; Bear, J. C.; Subramani, R. Multi-walled carbon nanotubes (MWCNTs)-reinforced ceramic nanocomposites for aerospace applications: a review. *Journal of Materials Science* **2022**, *57* (6), 3923-3953.
(23) Garcia, J.; Caffrey, E.; Doolan, L.; Horvath, D. V.; Carey, T.; Gabbett, C.; Coleman, J. N. Near Room Temperature Production of Segregated Network Composites of Carbon Nanotubes and Regolith as Multifunctional, Extra-Terrestrial Building Materials. *Small* **2024**, 2310954.
(24) Geng, Z.; Zhang, L.; Wu, Z.; Huang, J.; Wang, X.; Tan, M. J.; She, W.; Zhou, H.; Geng, G. Silicate-lunar regolith composite: A vacuum self-hardened and comprehensively durable extraterrestrial construction material. *Construction and Building Materials* **2024**, *449*, 138517.
(25) Liao, H.; Zhu, J.; Chang, S.; Xue, G.; Pang, J.; Zhu, H. Lunar regolith-AlSi10Mg composite fabricated by selective laser melting. *Vacuum* **2021**, *187*, 110122.
(26) Tafsirojjaman, T.; Smith, S. T.; Hossain, M. A. Development of regolith-resin-composite (RRC) material for lunar construction. *Acta Astronautica* **2025**, *228*, 652-663.
(27) Bao, C.; Wang, Y.; Mushtaq, R. T.; Chen, X.; Liu, Z.; Li, X.; Liu, M. Preparation and characterization of elevated and cryogenic temperature-resistant regolith-based epoxy resin composites. *Construction and Building Materials* **2023**, *387*, 131560.
(28) Suhaizan, M. S.; Tran, P.; Exner, A.; Falzon, B. G. Regolith sintering and 3D printing for lunar construction: An extensive review on recent progress. *Progress in Additive Manufacturing* **2024**, *9* (6), 1715-1736.
(29) Warren, P.; Raju, N.; Ebrahimi, H.; Krsmanovic, M.; Raghavan, S.; Kapat, J.; Ghosh, R. Effect of sintering temperature on microstructure and mechanical properties of molded Martian and Lunar regolith. *Ceramics International* **2022**, *48* (23), 35825-35833.
(30) Han, W.; Zhou, Y.; Cai, L.; Zhou, C.; Ding, L. Physical, mechanical and thermal properties of vacuum sintered HUST-1 lunar regolith simulant. *International Journal of Mining Science and Technology* **2024**.
(31) Abushama, W. J.; Tamimi, A. K.; Tabsh, S. W.; El-Emam, M. M.; Ibrahim, A.; Mohammed Ali, T. K. Influence of Optimum Particle Packing on the Macro and Micro Properties of Sustainable Concrete. *Sustainability* **2023**, *15* (19), 14331.
(32) Fennis, S.; Walraven, J. C.; Den Uijl, J. A. The use of particle packing models to design ecological concrete. *Heron* **2009**, *54* (2/3), 185-204.

(33) Shi, J.; Xiao, Z.; Xiao, Y.; Liu, H. Bio-molding of Lunar Regolith with Bio-carbonized Magnesium Oxide. *Biogeotechnics* **2024**, 100159.
(34) Prater, J.; Kim, Y. H. Carbon Nanotube Reinforced Lunar-Based Geopolymer: Curing Conditions. *Journal of Composites Science* **2024**, *8* (12), 492.
(35) Mandell, D. J.; Chorny, I.; Groban, E. S.; Wong, S. E.; Levine, E.; Rapp, C. S.; Jacobson, M. P. Strengths of hydrogen bonds involving phosphorylated amino acid side chains. *Journal of the American Chemical Society* **2007**, *129* (4), 820-827.
(36) Wei, L.; Liu, X.; Gao, Y.; Lv, X.; Hu, N.; Chen, M. Synergistic strengthening effect of titanium matrix composites reinforced by graphene oxide and carbon nanotubes. *Materials & Design* **2021**, *197*, 109261.
(37) Awadallah-f, A.; Al-Muhtaseb, S. Carbon nanoparticles-decorated carbon nanotubes. *Scientific Reports* **2020**, *10* (1), 4878.
(38) Garzon-Roman, A.; Ferreiro, A.; Zúñiga-Islas, C.; Rabanal, M. E. Evaluation of synthesis time in the growth of vertical-aligned MWCNTs by spray pyrolysis. *Materials Characterization* **2023**, *203*, 113105.
(39) Li, Z.; Corr, D. J.; Han, B.; Shah, S. P. Investigating the effect of carbon nanotube on early age hydration of cementitious composites with isothermal calorimetry and Fourier transform infrared spectroscopy. *Cement and Concrete Composites* **2020**, *107*, 103513.
(40) Liu, X. IR Spectrum and Characteristic Absorption Bands. Organic Chemistry I ed.
(41) Voropaev, S. Moon's Formation from Gas-Dust Cloud: New Geochemical and Astronomical Data. In *Advances in Geochemistry, Analytical Chemistry, and Planetary Sciences: 75th Anniversary of the Vernadsky Institute of the Russian Academy of Sciences*, Springer, 2023; pp 365-374.
(42) Collins, P. J.; Edmunson, J.; Fiske, M.; Bilén, S. G.; Radlińska, A. Geopolymer Lunar Concrete under Reduced-Pressure Curing and Vacuum Exposure. In *73rd International Astronautical Congress*, 2022.
(43) Shirasu, K.; Yamamoto, G.; Tamaki, I.; Ogasawara, T.; Shimamura, Y.; Inoue, Y.; Hashida, T. Negative axial thermal expansion coefficient of carbon nanotubes: Experimental determination based on measurements of coefficient of thermal expansion for aligned carbon nanotube reinforced epoxy composites. *Carbon* **2015**, *95*, 904-909.
(44) Tsou, C.; Huang, Y.-S.; Li, H.-C.; Lai, T.-H. Determination of thermal expansion coefficient of thermal oxide. *Sens. Mater* **2005**, *17* (11).
(45) Bobzin, K.; Kalscheuer, C.; Möbius, M. P.; Aghdam, P. H. Thermal stability of thick α-and γ-Al2O3 coatings deposited by high-speed PVD. *Surface and Coatings Technology* **2024**, *477*, 130411.
(46) De Almeida, M.; Brook, R.; Carruthers, T. Thermal expansion of ceramics in the MgO-CaO system. *Journal of Materials Science* **1979**, *14*, 2191-2194.
(47) Bezerra, U.; Alves, S.; Barbosa, N.; Torres, S. Corpo de prova na forma de ampulheta: resistência à compressão de concretos e argamassas (análises numérica e experimental). *Revista IBRACON de estruturas e materiais* **2016**, *9*, 510-524.
(48) Girish, H.; Balaji, N. The Failure Behaviour of Concrete Cubes in Compression. In *International Conference on Sustainable Infrastructure: Innovation, Opportunities and Challenges*, 2023; Springer: pp 151-162.
(49) Shercliff, H.; Ashby, M. Elastic structures in design. *Encyclopedia of Materials: Science and Technology* **2001**, 2429-2433.

(50) Schodek, D. L.; Ferreira, P.; Ashby, M. F. *Nanomaterials, nanotechnologies and design: an introduction for engineers and architects*; Butterworth-Heinemann, 2009.
(51) Gorkina, A. L.; Tsapenko, A. P.; Gilshteyn, E. P.; Koltsova, T. S.; Larionova, T. V.; Talyzin, A.; Anisimov, A. S.; Anoshkin, I. V.; Kauppinen, E. I.; Tolochko, O. V. Transparent and conductive hybrid graphene/carbon nanotube films. *Carbon* **2016**, *100*, 501-507.
(52) Shah, D. U. Materials Selection Charts for Designing Products With Biocomposites. **2020**.
(53) Malla, R. B.; Brown, K. M. Determination of temperature variation on lunar surface and subsurface for habitat analysis and design. *Acta Astronautica* **2015**, *107*, 196-207.
(54) Williams, D. Moon Fact Sheet. NASA.

This study investigated the impact of MWCNT reinforcement on the compressive strength of lunar regolith composites under varied curing conditions, including ambient with and without cycling and vacuum with cycling. Utilizing experimental methodologies, it identified significant relationships between MWCNT content, curing protocols, and thermal cycling, providing insights into optimizing durability and addressing thermal mismatch for resource-efficient lunar habitat construction.

Supporting Information

Balancing Strength and Extreme Thermal Resilience in Lunar Regolith Composites: The Role of Multi-Walled Carbon Nanotubes

*Andrea J. Hoe, Amirreza Tarafdar, Wenhua Lin, Michael R. Fiske, Jennifer Edmunson, Yeqing Wang**

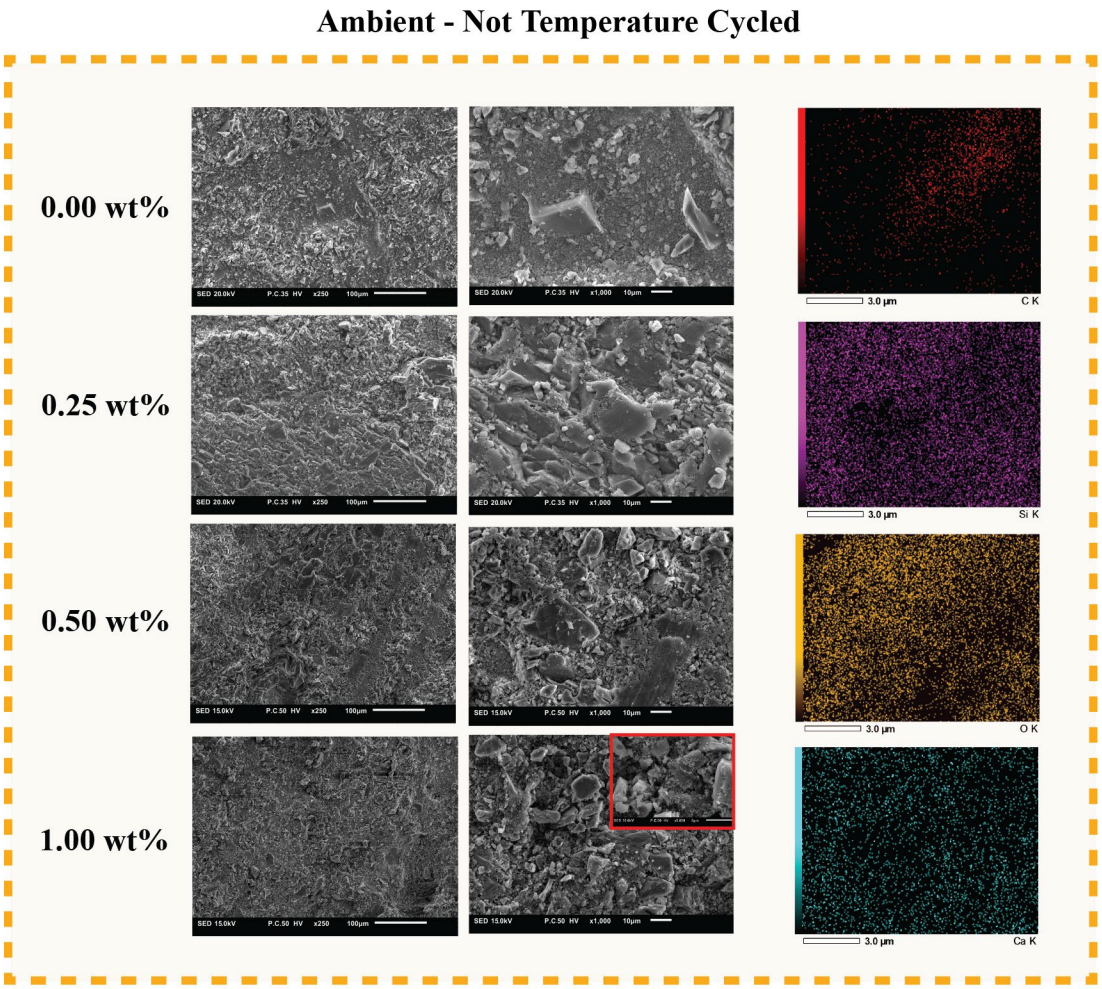

Figure S1: SEM images of each MWCNT wt% sample under ambient conditions without temperature cycling are presented in the left column, captured at two magnification levels. The

4.00 wt% MWCNT sample is highlighted and further magnified for detailed analysis. EDS images of the 1.00 wt% MWCNT sample are shown in the right column.

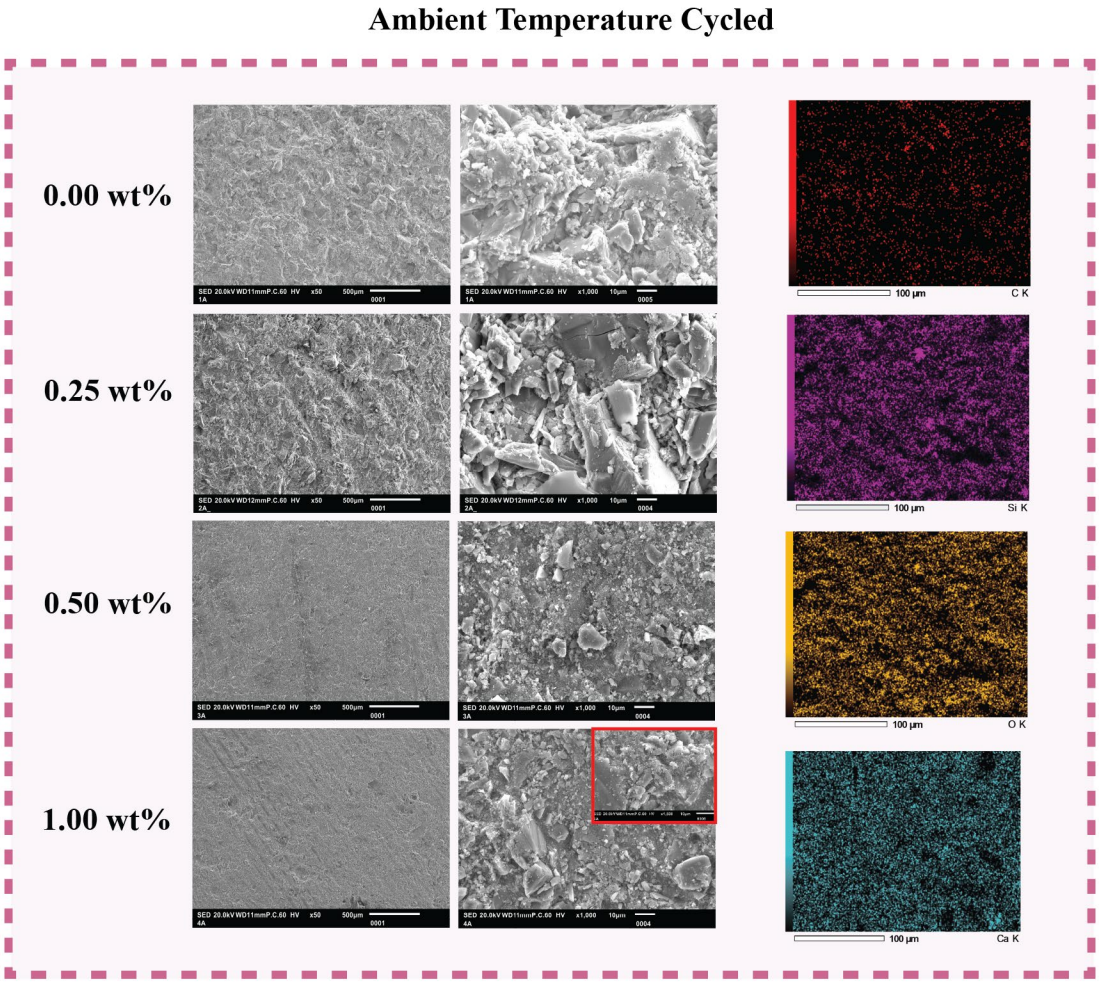

Figure S2: SEM images of each MWCNT wt% sample under ambient conditions with temperature cycling are presented in the left column, captured at two magnification levels. The 4.00 wt% MWCNT sample is highlighted and further magnified for detailed analysis. EDS images of the 1.00 wt% MWCNT sample are shown in the right column.

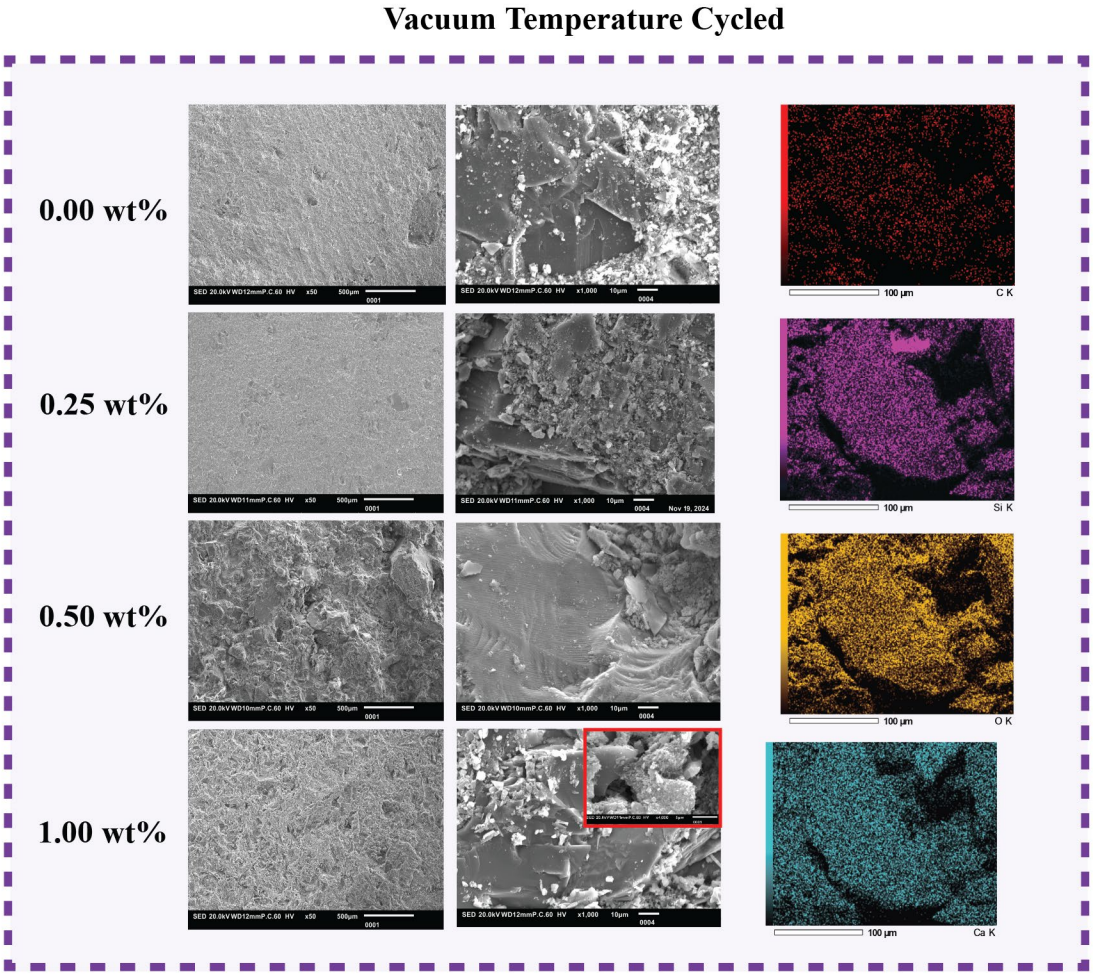

Figure S3: SEM images of each MWCNT wt% sample under vacuum conditions with temperature cycling are presented in the left column, captured at two magnification levels. The 4.00 wt% MWCNT sample is highlighted and further magnified for detailed analysis. EDS images of the 1.00 wt% MWCNT sample are shown in the right column.

Table S1. Material Properties of Lunar Regolith and MWCNT for the Simulation

	Density [kg/m³]	CTE [1/K]	CTC [W/m·K]	Specific heat [J/kg.K]	Elastic modulus [GPa]	Poisson's ratio
Lunar	3120[a)]	1.04×10^{-6}[b)]	11.25[c)]	668.69[d)]	85[e)]	0.2[f)]
MWCNT	2100[g)]	-1.20×10^{-5}[h)]	3000[i)]	550[j)]	500[k)]	0.2[l)]

[a)]Ref.[1, 2] ; [b)]Ref.[1-4]; [c)]Ref.[1, 2, 5-8]; [d)]Ref.[2, 5, 9-12]; [e)]Ref.[1, 2]; [f)]Ref.[1, 2] ; [g)]Ref.[13]; [h)]Ref.[14]; [i)]Ref.[15, 16]; [j)]Ref.[13]; [k)]Ref.[17]; [l)]Ref.[18]

(1) Materials, A. *Silica - Silicon Dioxide (SiO2)*. 2001. https://www.azom.com/article.aspx?ArticleID=1114 (accessed).
(2) *Alumina - Aluminium Oxide - Al2O3 - A Refractory Ceramic Oxide*. 2001. https://www.azom.com/article.aspx?ArticleID=52 (accessed 2025 Jan. 15).
(3) *Older Glass Thermal Expansion Models*. https://glassproperties.com/expansion/Old-Thermal-Expansion-Models.htm#:~:text=Go%20to:%20Contemporary%20Glass%20Thermal,according%20to%20Winkelmann%20and%20Schott. (accessed).
(4) Seagle, C.; Heinz, D.; Campbell, A.; Prakapenka, V.; Wanless, S. Melting and thermal expansion in the Fe–FeO system at high pressure. *Earth and Planetary Science Letters* **2008**, *265* (3-4), 655-665.
(5) Takeda, M.; Onishi, T.; Nakakubo, S.; Fujimoto, S. Physical properties of iron-oxide scales on Si-containing steels at high temperature. *Materials transactions* **2009**, *50* (9), 2242-2246.
(6) Li, M.; Endo, R.; Akoshima, M.; Tanei, H.; Okada, H.; Susa, M. Thermal conductivity of oxide scale thermally grown on iron substrate corrected by temperature-dependent interfacial thermal resistance in laser flash measurement. *ISIJ International* **2019**, *59* (3), 398-403.
(7) Yan, X.; Cao, W.; Li, H. Thermal transport properties of Na2X (X= O and S) monolayers. *Coatings* **2022**, *12* (9), 1294.
(8) Abdelmalik, A.; Sadiq, A. Thermal and electrical characterization of composite metal oxides particles from periwinkle shell for dielectric application. *SN Applied Sciences* **2019**, *1* (4), 373.
(9) Zhu, W.; Zheng, G.; Cao, S.; He, H. Thermal conductivity of amorphous SiO2 thin film: A molecular dynamics study. *Scientific reports* **2018**, *8* (1), 10537.
(10) *Sodium Oxide*. https://webbook.nist.gov/cgi/cbook.cgi?ID=C12401864&Type=JANAFG&Table=on (accessed).
(11) *Iron Oxide*. https://webbook.nist.gov/cgi/cbook.cgi?ID=C1345251&Mask=2&Type=JANAFS&Table=on (accessed 2025 Jan. 15).
(12) *Calcium Oxide*. https://webbook.nist.gov/cgi/cbook.cgi?ID=C1305788&Mask=2&Type=JANAFS&Plot=on (accessed 2025 Jan. 15).
(13) Alizadeh, H.; Pourpasha, H.; Heris, S. Z.; Estellé, P. Experimental investigation on thermal performance of covalently functionalized hydroxylated and non-covalently functionalized multi-walled carbon nanotubes/transformer oil nanofluid. *Case Studies in Thermal Engineering* **2022**, *31*, 101713.
(14) Lincon, M. I.; Chalivendra, V. B. Dynamic mode-I fracture toughness and damage sensing characterization in additively manufactured ABS nanocomposites. *The International Journal of Advanced Manufacturing Technology* **2024**, 1-16.

(15) Fikri, M. A.; Pandey, A.; Samykano, M.; Kadirgama, K.; George, M.; Saidur, R.; Selvaraj, J.; Abd Rahim, N.; Sharma, K.; Tyagi, V. Thermal conductivity, reliability, and stability assessment of phase change material (PCM) doped with functionalized multi-wall carbon nanotubes (FMWCNTs). *Journal of Energy Storage* **2022**, *50*, 104676.
(16) Chua, T.; Mariatti, M.; Azizan, A.; Rashid, A. Effects of surface-functionalized multi-walled carbon nanotubes on the properties of poly (dimethyl siloxane) nanocomposites. *Composites science and technology* **2010**, *70* (4), 671-677.
(17) Li, Y.; Li, H.; Jin, C.; Wang, Z.; Hao, J.; Li, Y.; Liu, J. Multi-scale investigation and mechanism analysis on Young's modulus of CSH modified by multi-walled carbon nanotubes. *Construction and Building Materials* **2021**, *308*, 125079.
(18) Miao, M.; McDonnell, J.; Vuckovic, L.; Hawkins, S. C. Poisson's ratio and porosity of carbon nanotube dry-spun yarns. *Carbon* **2010**, *48* (10), 2802-2811.